Quantifying the Dependence of Satellite Cloud Retrievals on Changes in Instrument Calibration

Yolanda L. Shea* and Bruce A. Wielicki

NASA Langley Research Center, Hampton, Virginia

Sunny Sun-Mack

Science Systems and Applications Inc, Hampton, Virginia

Patrick Minnis

NASA Langley Research Center, Hampton, Virginia

Corresponding author address: NASA Langley Research Center, Mail Stop 420, Hampton, VA, USA.

E-mail: yolanda.shea@nasa.gov

ABSTRACT

How clouds will respond to Earth's warming climate is the greatest contributor to intermodel spread of Equilibrium Climate Sensitivity (ECS). Although global climate models (GCMs) generally agree that the total cloud feedback is positive, GCMs disagree on the magnitude of cloud feedback. Satellite instruments with sufficient accuracy to detect climate change-scale trends in cloud properties will provide improved confidence in our understanding of the relationship between observed climate change and cloud property trends, thus providing essential information to better constrain ECS. However, a robust framework is needed to determine what constitutes sufficient or necessary accuracy for such an achievement. Our study applies a climate change accuracy framework to quantify the impact of absolute calibration accuracy on climate change-scale trend detection times for cloud fraction, effective temperature, optical thickness, and effective radius. With this framework, we demonstrate how more stringent absolute accuracy requirements for reflected solar and infrared cloud imagers enable improved constraint of SW and LW cloud feedbacks and the ECS by significantly reducing trend uncertainties for cloud fraction, optical thickness, and effective temperature compared to operational instruments. Additionally, more stringent absolute accuracy requirements compared to today's operational instruments would help to further constrain the aerosol indirect effect, the largest uncertainty in radiative forcing, by reducing water cloud effective radius trend uncertainty. This study demonstrates the application of this climate accuracy framework and the implications of its results within climate science.

1. Introduction

Clouds play a significant role in the Earth's radiation budget by modulating the magnitude of shortwave (SW) reflected (0.3 μm–3.5 μm) and longwave (LW) emitted (3.5 μm–100 μm) radiation at the top of the atmosphere (TOA) (Stephens et al. 1990; Chen et al. 2000; Stephens 2005). On a global, annual scale, clouds reduce incoming SW (outgoing LW) irradiance by about 50 Wm^{-2} (28 Wm^{-2}). Clouds, therefore, have a net cooling effect on Earth's climate system of about 22 Wm^{-2}, according to the CERES EBAF-TOA (Clouds and Earth's Radiant Energy System Energy Balance and Filled) data set (Loeb et al. 2009, 2012; Dolinar et al. 2014). Changes in cloud macrophysical (e.g. height, amount) and microphysical (e.g. optical thickness, effective particle size) properties induce positive (amplifying) or negative (dampening) feedbacks, thus contributing to the Earth's climate system response to climate forcings and non-cloud feedbacks.

How clouds will respond to Earth's warming climate is one of the largest sources of uncertainty among Global Climate Model (GCM) projections. Net cloud feedbacks in modeling experiments comprising the fifth phase of the Climate Model Intercomparison Project (CMIP5) (Taylor et al. 2012) tend to be nearly neutral or positive meaning that CMIP5 models predict that clouds will likely change such that they will cool the planet less as global mean surface temperature increases. However, a significant amount of disagreement remains regarding the magnitude of the net cloud feedback among CMIP5 model output (Flato et al. 2013). Estimating SW and LW cloud feedback from observations requires global monitoring of observed decadal changes in the SW and LW cloud radiative effect (CRE) (previously, cloud forcing), the difference between clear-sky and all-sky TOA irradiance (flux). Understanding the physical basis of CRE decadal trends requires a comprehensive understanding of how global cloud properties that govern trends in SW and LW CRE respond to changes in Earth's climate.

The uncertainty in CMIP5 SW cloud feedback is the largest contributor to intermodel spread in equilibrium climate sensitivity (ECS) (2.1K to 4.7K), a range that remains similar to that previously reported from the CMIP3 modeling experiments (Flato et al. 2013). This raises the question of what is needed to better constrain cloud feedback and therefore ECS. The tools used to observe Earth's climate system must have the required accuracy to detect cloud property trends on climate change-relevant scales (>2000 km spatial and decadal temporal scales). Included among these tools are passive remote sensing satellite measurements and the associated retrieval algorithms used to infer macrophysical and microphysical cloud properties from those measurements. The accuracy of both the satellite instruments and algorithms must be sufficient for unambiguous understanding of cloud response to climate change.

Climate change detection requires measurements from instruments with high accuracy that provide the capability to detect what are likely to be small, global and inter-annual changes within Earth's climate system (Ohring et al. 2005). Wielicki et al. (2013) addressed the challenge of robustly and quantitatively defining climate change accuracy requirements by developing an accuracy framework that can be applied to a diverse swath of Essential Climate Variables (ECVs) and measurement systems to determine the necessary accuracy requirements of a satellite-based observing system (Leroy et al. 2008; Weatherhead et al. 1998). This accuracy framework provides a quantitative basis for determining climate science-driven accuracy requirements for a diversity of satellite instruments and geophysical variables.

Wielicki et al. (2013) presented this accuracy framework using, as an example, the Climate Absolute Radiance and Refractivity Observatory (CLARREO), a Tier-1 Decadal Survey-recommended climate observing mission (National Research Council 2007). The CLARREO mission concept includes reflected solar (RS) and infrared (IR) spectrometers with SI-traceable on-orbit calibration designed to achieve substantially higher accuracy, up to ten times greater, than

any currently or previously operational Earth-observing satellite sensor. These instruments will be used both for climate benchmarking and inter-calibrating with other instruments that are operational during the CLARREO lifetime. CLARREO inter-calibration would include cloud imagers, such as MODIS (Moderate Resolution Imaging Spectroradiometer) and VIIRS (Visible/Infrared Imager/Radiometer Suite), thus enabling the improved accuracy of the reflectance and brightness temperature measurements used in their corresponding geophysical retrieval algorithms. During its inter-calibration activities, the CLARREO instruments would serve as calibration standards in orbit, with the ability to improve the accuracy of up to 30-40 currently operational satellite instruments in low-Earth and geostationary orbit (Roithmayr et al. 2014a,b).

The satellite sensors with which the CLARREO instruments would inter-calibrate would still be essential parts of the global climate observing system. For example, cloud imagers have the spatial and temporal sampling needed for global monitoring of cloud properties, and the CERES instruments have the angular sampling required to estimate TOA SW and LW irradiance (flux). The CLARREO mission goals of unprecedented accuracy and high information content for inter-calibration and climate benchmarking allow for the mission to contribute to the climate community's needs independently and in conjunction with the other essential instruments within the climate observing system. In our studies, we will also apply the accuracy framework using the CLARREO requirements as examples of climate mission requirements.

Wielicki et al. (2013) (hereafter, *W13*) presented an accuracy framework to quantify climate change instrument requirements based on the need to detect global mean trends in two ECVs: the SW cloud radiative effect and global mean surface temperature. W13 illustrated the importance of high instrument accuracy for constraining trend detection times for these two ECVs. However, the impact of instrument and algorithm uncertainties on delaying trend detection times in many other ECVs remains to be evaluated. This includes cloud properties, which, as we have noted above, are

a crucial, but largely uncertain part of understanding observed climate changes and constraining the spread among climate model projections.

Other studies have applied this framework to study the effect of measurement errors on precipitable water vapor trend detection times (Roman et al. 2014), to compare the trend detection times between RS hyperspectral and broadband climate Observing System Simulation Experiment (OSSE) simulations (Feldman et al. 2011), and to quantify the IR spectral fingerprinting retrieval error impact on atmospheric and cloud property trend uncertainties (Kato et al. 2014). The versatility of this framework allows for its application to a wide array of observing systems and ECVs.

In this study, we apply the principles of the W13 accuracy framework to evaluate the impact of reflected solar and infrared instrument accuracy requirements on trend uncertainty and trend detection time of satellite-retrieved cloud properties. We focus our studies on absolute calibration instrument accuracy, which dominates trend uncertainty on global scales; although other noise and uncertainty sources also contribute to trend uncertainty (W13).

The analysis described herein was conducted using cloud properties retrieved from the CERES (Wielicki et al. 1996) Cloud Property Retrieval System (CPRS) (Minnis et al. 2011) which ingests spatially subsetted MODIS reflectance and brightness temperatures. We therefore quantified the MODIS-like accuracy requirements needed to observe climate change trends in retrieved cloud properties. This analysis is the first of its kind.

In Section 2, we describe the W13 climate accuracy framework used in this study. Section 3 includes the details of how we applied the framework in our analysis of cloud properties. In Section 4 we present our analysis of the results and their implications, and in Section 5 we summarize our studies, present our conclusions, and discuss future work.

2. Climate Observing System Accuracy Framework

W13 demonstrated a climate observing system accuracy framework based on earlier work by Leroy et al. (2008) and Weatherhead et al. (1998). Leroy et al. (2008) derived the following equation to calculate the trend uncertainty, δm, for a geophysical variable as determined from a measured time series of record length Δt:

$$\delta m = \sqrt{12\Delta t^{-3}(s_n\sigma_{var})^2\kappa_{var} + (s_n\sigma_{Vcal})^2\kappa_{cal})}, \quad (1)$$

where σ_{var} is the standard deviation of natural variability, κ_{var} is the autocorrelation time of natural variability, σ_{Vcal} is the calibration uncertainty of the geophysical variable, κ_{cal} is the calibration autocorrelation time, and s_n is the signal-to-noise ratio (e.g. $s_n = 2$ for a 95% confidence bound). Autocorrelation time can be thought of as the amount of time between independent measurements and is a function of the lag-1 autocorrelation (Weatherhead et al. 1998). As shown in W13, additional uncertainties can be evaluated using Eqn. 1, such as instrument noise and orbit sampling uncertainty. As discussed in Section 1, however, calibration uncertainty tends to dominate the trend uncertainty (among instrument noise, calibration, and sampling uncertainty) of geophysical variables on global scales (W13); therefore, we focus in this paper on absolute calibration uncertainty for global trends of cloud properties. The calibration autocorrelation time can be understood as the time over which the calibration of the instrument can be assumed to drift within the instrument's calibration uncertainty. Units of δm are dependent upon the units of the uncertainties, autocorrelation times, and record length. Consistent units should be used for natural variability and calibration uncertainty, as well as for record length and autocorrelation time.

The trend uncertainty determined from measurements made by a perfect instrument, δm_p, is only limited by the natural variability of the climate variable, as shown in Eqn. 2 (Leroy et al. 2008). Regardless of how flawless an instrument may be, it cannot be used to detect an anthro-

pogenic trend in the climate system with uncertainty less than that caused by natural (internal) variability (due to, e.g. El Niño or volcanic eruptions).

$$\delta m_p = \sqrt{12\Delta t^{-3}(s_n\sigma_{var})^2\kappa_{var}} \tag{2}$$

In the current paper, we use σ_{var} as the standard deviation of the variable's global, annual mean time series. The presence of a trend in a time series used to estimate σ_{var} can artificially increase both natural variability parameters, which would lead to erroneously less stringent instrument accuracy requirements. For κ_{var}, we use the Weatherhead et al. (1998) definition, $\kappa_{var} = \sqrt{(1+\rho_1)/(1-\rho_1)}$, where ρ_1 is the lag-1 autocorrelation of the anomaly time series. Details of determining the natural variability (σ_{var} and κ_{var}) specific to the cloud properties examined in these studies are discussed in Section 3. Phojanamongkolkij et al. (2014) found only small differences in trend uncertainty estimation using the Weatherhead et al. (1998) versus (Leroy et al. 2008) definition of autocorrelation time and in using monthly versus annual time series.

Information in Eqns. 1 and 2 can be used to determine a calibration uncertainty requirement, depending on how close to perfect it is desired for an observing system to be capable of detecting a trend, a concept that can be quantified by taking the ratio between δm and δm_p.

$$U_a = \frac{\delta m}{\delta m_p} = \sqrt{1 + \frac{(s_n\sigma_{Vcal})^2\kappa_{cal}}{(s_n\sigma_{var})^2\kappa_{var}}} \tag{3}$$

In these studies, we assumed a standard satellite instrument lifetime of 5 years for the calibration autocorrelation time, κ_{cal}, and set a goal for the RS and IR CLARREO instruments to be 20% from perfect, making $U_a = 1.2$. This goal means that these instruments would be designed such that the geophysical trends would be no more than 20% more uncertain than those trends calculated using a perfect instrument.

Solving Eqn. 3 for σ_{Vcal}, we obtain the required absolute calibration to satisfy the trend uncertainty goal, indicated by the value of U_a.

$$s_n \sigma_{Vcal} = \sqrt{\frac{(U_a^2 - 1)(s_n \sigma_{var})^2 \kappa_{var})}{\kappa_{cal}}} \tag{4}$$

Note that σ_{Vcal} is in the units of the cloud variable (or whichever geophysical variable is being studied), not calibrated instrument units such as reflectance or brightness temperature. Also, because ultimately the calibration instrument accuracy will be reported for some signal-to-noise ratio or confidence level, we included s_n on the left side of the equation as well. To determine σ_{cal}, the measurement uncertainty in calibrated instrument units, we need to characterize the relationship between each cloud property and reflectance or brightness temperature in the MODIS spectral bands used to retrieve those cloud properties, analysis for which we provide details in Section 3b. The examples for calibration requirements provided by W13 used temperature and shortwave cloud radiative forcing (effect) as the geophysical climate variables. In those cases, there is a simple direct relationship between instrument calibration and each geophysical variable. For cloud properties, the relationship is less direct and requires the additional analysis shown in Sections 3 and 4.

3. Determining Requirements from Accuracy Framework

a. Natural Variability of CERES/MODIS Cloud Properties

We examine several cloud properties retrieved by the CERES (Wielicki et al. 1996) Cloud Property Retrieval System (CPRS) (Minnis et al. 2011): cloud fraction, cloud optical thickness ($\log_{10}$), liquid water cloud effective radius, and cloud effective temperature. The logarithm of optical

thickness was evaluated because it is approximately linearly proportional to the cloud radiative effect.

To estimate the natural variability parameters, σ_{var} and κ_{var}, globally and annually averaged cloud property anomaly time series were constructed from the CERES/MODIS SSF1deg Edition 4A Cloud Products (Wielicki et al. 1996; Minnis et al. 2011) using 11 years of data between July 2002 and June 2013. These averages excluded regions poleward of 60° N and S and any 1° grid boxes containing snow or ice identified using the 1° CERES monthly compilation of snow and ice percent coverage of the National Snow and Ice Data Center's 25 km daily coverage (Nolin et al. 1998) and the permanent snow map from the U.S. Geological Survey's International Geosphere/Biosphere Programme (IGBP) (Loveland et al. 2000). The cloud mask algorithm operates differently when discriminating clouds from snow or ice-covered surfaces (Trepte et al. 2003; Minnis et al. 2008), so these regions were eliminated to focus the scope of these studies.

Because MODIS Terra sensor degradation has contributed to calibration-based trend artifacts in geophysical properties retrieved from the MODIS TERRA L1B data (Lyapustin et al. 2014) we used the CERES/MODIS Aqua cloud properties to compute σ_{var} and κ_{var}. This study was conducted on global and annual scales to provide the most stringent spatial and temporal constraint on accuracy requirements. Natural variability increases at smaller zonal and regional scales compared to global and annual scales, resulting in less stringent requirements (Wielicki et al. 2013). A second reason to use global means is that cloud feedback is most closely related to global mean changes in cloud properties (Zelinka et al. 2012, 2013).

Using linear regression, we de-trended the time series prior to calculating σ_{var} and κ_{var} to remove any significant linear trends, which would artificially inflate both terms. Lastly, using currently available observed time series of cloud properties to determine their natural variability results in short annual time series (11 years). The σ_{var} of short times series tends to be underestimated.

To address this, we used the Student-t statistical distribution to scale the standard deviation using the degrees of freedom of our problem, rather than the Student-t value for an infinite number of samples. This has an impact on the $s_n\sigma_{var}$ and $s_n\sigma_{Vcal}$ products found in the equations above. For example, rather than calculate the 95% confidence calibration uncertainty by using $s_n = 2$, we use the Student-t value for 10 degrees of freedom of $s_n = 2.228$.

The natural variability parameters of the cloud properties evaluated in this study are shown in Table 1. For calculating requirements in the reflected solar bands, σ_{var} values were calculated relative to the 11-year cloud property averages, which are also shown in Table 1.

b. Sensitivity of CPRS Cloud Properties to Instrument Changes

Using Eqn. 4, σ_{Vcal} (absolute and relative) was calculated for each cloud property, shown in the last two columns of Table 1. σ_{cal}, the absolute calibration requirement in calibrated measurement units (reflectance and brightness temperature) must ultimately be computed, however, using the following relationship:

$$\sigma_{Vcal} = \sigma_{cal}\frac{\partial C}{\partial I} \tag{5}$$

where C is the cloud property of interest (e.g. cloud fraction, optical thickness), and I is the measurement in calibrated instrument units (reflectance or brightness temperature). We used the offline CERES Cloud Property Retrieval System (CPRS) Edition 4 with the CERES clear-sky start-up maps to calculate the sensitivity of the cloud properties to small changes in reflectance and brightness temperature (BT) to the primary MODIS Aqua channels used in the daytime (SZA $< 82^\circ$), non-polar (60°S to 60°N) cloud retrievals: 0.65 μm, 3.79 μm, 11 μm, 12 μm.

The reflectance in the 0.65 μm band was changed by $\pm$0.3% and $\pm$1%, and the BT in the 3.79 μm, 11 μm, and 12 μm bands were each changed by $\pm$0.3 K and $\pm$1 K. Gain changes were

applied in the RS band and offset changes were applied in the IR bands to emulate the type of calibration drifts expected in comparable RS and IR instruments. We calculated the absolute and relative differences between each cloud property after each individual calibration change in each band and the values from the baseline run, wherein no calibration changes were imposed.

As in the natural variability analysis, snow or ice-covered pixels in non-polar regions were excluded from this sensitivity analysis. These sensitivity studies were conducted using the highest resolution of MODIS data available at the NASA Langley Atmospheric Science Data Center (ASDC), which is subsampled to every other pixel and every other scan line from the 1km MODIS L1B data. This results in MODIS reflectance and BT at a 1 km resolution and 2 km spatial sampling. Additionally, since MODIS is a passive instrument, only clouds with an optical thickness of at least 0.3 were included in these studies.

Tests were conducted to determine the number of samples sufficient for robust statistics of cloud property sensitivity to reflectance and BT. The files for each day contain on the order of 10^6 cloud pixels. Given the large number of CPRS runs needed, we determined an appropriate subset of days within a month (in our case, July 2003), such that the averaged change in each cloud property was representative of the average computed using a full month's worth of data. We explored this using a subset of our planned CPRS sensitivity runs: the gain increases imposed upon the 0.65 μm band MODIS reflectance for the entire month of July 2003. We calculated the requirements for the 0.65 μm channel for each cloud property using differenced averages that included an increased number of days throughout the month, starting with the first day of July 2003. The final calculation for the month were differenced averages computed using the cloud data for the entire month. We found that by the three-week mark (21 days), the requirements for each cloud property stabilized to a value that was typically 4% or less than the full month value. The only deviation we saw from this

difference was a 10% relative difference from the full month value for cloud fraction. We therefore decided to use 21-day averages for the remainder of our studies.

In setting up such studies, one should also consider the other design aspects of the new instrument. For example, the CLARREO Reflected Solar spectrometer has been designed to match measurements with other sensors in space, time, and viewing angle (W13), meaning that the CLARREO Reflected Solar instrument design allows for inter-calibrating with a MODIS-like instrument across its full swath. We therefore evaluated cloud properties retrieved across the MODIS full swath.

Global, 21-day cloud property means were calculated using MODIS data from the first three weeks of July 2003. Linear regression was applied to determine the slope for each set of absolute and relative differenced averages. Because both positive and negative calibration changes were imposed, the linear parameters for both sets of changes were computed separately. This allowed examination of linearity for every band, imposed change, and cloud property across both the negative and positive changes. The slopes determined from the linear regressions give the averaged sensitivity of each cloud property (C in Eqn. 5) to changes in MODIS reflectance or brightness temperature (I in Eqn. 5). The standard deviations of the daily, globally averaged differences were used to determine the uncertainties in the regression slopes, allowing for estimation of the uncertainty in the sensitivities, and, ultimately the determined requirements.

Upon calculating the requirements for each cloud property and each band it was clear that certain cloud property-driven requirements served as limiting factors within each spectral band. Five of these sensitivities (slopes) are shown in Table 2 for the band(s) predominantly used to calculate each property: cloud optical thickness (0.65 μm), cloud fraction (11 and 12 μm), effective cloud temperature (11 μm), and water droplet effective radius (3.8 μm). The sensitivities shown in Table 2 are the average sensitivities determined from the linear regressions discussed above. In these

cases discussed here, the relationships were linear across the increased and decreased changes, as shown in Figure 1 with two examples: cloud optical depth and effective temperature.

The bands shown in Table 2 are not the only bands to which these four cloud properties were sensitive. For example, the CPRS cloud mask is determined prior to calculating cloud optical depth using the 0.65μm reflectance ($R_{0.65\mu m}$), so although the optical depth is predominantly sensitive to changes in the $R_{0.65\mu m}$, it is also sensitive to changes in the 11 and 12 μm brightness temperatures ($BT_{11\mu m}$ and $BT_{12\mu m}$). Information in both of those bands is used in the cloud mask, changes in which will, to some degree, impact the average magnitude of the cloud optical depth and other subsequently retrieved cloud properties.

For simplicity and to clearly demonstrate a proof of concept for applying the climate accuracy framework to cloud properties retrieved from cloud imagers, we have conducted these studies by considering changes in each band individually. Evaluating changes in multiple bands simultaneously remains for future study and would more realistically simulate potential changes in an operational satellite instrument.

The results from these studies are dependent on the algorithm used. Alternate results can be expected if a different algorithm (MODIS-ST cloud algorithms) or cloud imager and its corresponding algorithms (e.g. VIIRS) were used to determine these sensitivities.

4. Implications for Instrument Requirements

a. Optical Thickness, Effective Temperature, and Cloud Fraction

Combining the natural variability and sensitivity results allows for calculation of instrument requirements (Eqns. 4 and 5). Using the initial CLARREO goal to design an instrument capable of detecting trends with uncertainties no more than 20% ($U_a = 1.2$) from that of a perfect instrument

(W13) as an example and starting point, we determined a relative σ_{var} for the $\log_{10}$ cloud optical thickness ($\log_{10}\tau_c$) of 0.621% and a κ_{var} of 0.85 years (Table 1). We then use Eqn. 4 to find $s_n\sigma_{Vcal}$ for $U_a = 1.2$. In this paper we discuss all requirements at 95% confidence (2σ); however, recall from Section 3a that we use $s_n = 2.228$ for a signal-to-noise ratio of 2 because of the tendency of shorter time series to underestimate variability. This resulted in a relative σ_{Vcal} of 0.170% (far right column of Table 1), and a $2\sigma_{Vcal}$ of 0.379% (i.e. at 95% confidence).

To compute the $2\sigma_{cal}$ value, we used Eqn. 5 and the relative sensitivity of the CERES/MODIS $\log_{10}\tau_c$ to $R_{0.65\mu m}$ gain changes, which we found to be 1.38 %/% (Table 2) (that is, percent relative $\log_{10}\tau_c$ to $R_{0.65\,\mu m}$). This gives an absolute calibration requirement for the 0.65μm band of 0.27%, nearly equivalent to the current CLARREO RS requirement of 0.3% (2σ) (W13). The 0.3% CLARREO RS broadband requirement was determined using the natural variability of the RS cloud radiative effect.

The time to detect relative $\log_{10}\tau_c$ trends for conceptual instruments with different calibration uncertainties using Eqn. 1, including a perfect instrument with an instrument calibration uncertainty of 0% (Eqn. 2) are shown in Figure 2. Figure 2a shows the length of time required to detect optical thickness trends at different trend uncertainty levels (at 95% confidence) using conceptual instruments with different calibration uncertainties in the 0.65 μm band. Figure 2b shows how much longer it would take to detect a trend in cloud optical thickness with an imperfect instrument (i.e. one with some calibration uncertainty) than it would with a perfect instrument (i.e. one limited only by natural variability).

Generally the detection times among different instruments span a larger range as the required trend uncertainty approaches 0 %/decade. For example, for an optical thickness trend of 10 %/decade the difference in detection time between a perfect observing system and one with a 3.6% (2σ) uncertainty spans about a decade, and a perfect observing system can observe such a

trend in less than 5 years. However, detection of a much smaller trend of 2 %/decade becomes more difficult, with detection time differences spanning about 25 years between a perfect observing system and one with 3.6% calibration uncertainty.

Without further information, however, the range of optical depth trend uncertainty shown in Figure 2 is arbitrary. The question that remains is over what range of trends our analysis should be focused. This can be determined by estimating the expected range of optical thickness trends that correspond to current climate model projections. Estimating this range would help to better constrain instrument accuracy requirements for detecting trends in optical thickness. To place these results into a climate change-relevant context, we related the cloud optical thickness trend to equilibrium climate sensitivity (ECS) and SW Cloud Feedback. Relating cloud feedback and ECS allows a focus on cloud optical thickness trends and cloud feedback magnitudes approximately corresponding to the Intergovernmental Panel on Climate Change (IPCC) Fifth Assessment Report (AR5) ECS intermodel range of 2.1 K to 4.7 K (Stocker et al. 2013).

We applied the forcing-feedback framework $\Delta\overline{RF} = \Delta\overline{ECS}\sum\bar{\lambda}_i$, using the IPCC AR5 Effective Radiative Forcing (RF) Fixed Sea Surface Temperature multi-model mean for doubled CO_2, $\Delta\overline{RF} = 3.7\,Wm^{-2}$. The non-cloud feedbacks were used from IPCC AR5 globally averaged model means of the Planck, water vapor, lapse rate, and surface albedo feedbacks (Flato et al. 2013), shown in Table 3.

The SW and LW cloud feedbacks used were the ensemble averages, neglecting rapid adjustments, calculated by Zelinka et al. (2013) from abrupt quadrupled CO_2 simulations, in which the cloud fraction, optical thickness, and altitude contributions to the SW and LW cloud feedbacks were partitioned by isolating contributions due to changes in cloud amount, cloud optical thickness, and cloud height using output from CFMIP2/CMIP5 model simulations and CTP-τ his-

tograms (Table 3). Using the $\Delta\overline{RF}$ and feedback values detailed above, we calculated an ECS of 2.53 K, which is within the AR5 intermodel range of 2.1 to 4.7 K (Stocker et al. 2013).

We used the forcing-feedback framework to calculate LW and SW cloud feedbacks solely due to changes in cloud amount, altitude, or optical depth for a range of equilibrium climate sensitivities. We describe our methodology of this process in detail using cloud optical thickness as an example. Using the AR5 $\Delta\overline{RF}$ for doubled CO_2, feedbacks listed in Table 3, and the range of ECS considered in this analysis, $(\Delta\overline{ECS})_j = 1-9\,K$, $\Delta ECS = 1\,K$, we computed nine corresponding values of the SW cloud feedback due to changes in cloud optical thickness, $\overline{\lambda}_{c,sw,\tau_c}$ with the following equation:

$$(\overline{\lambda}_{c,sw,\tau_c})_j = \frac{\Delta\overline{RF}}{(\Delta\overline{T}_s)_j} - \left\{\sum\bar{\lambda}_i - (\overline{\lambda}_{c,sw,\tau_c})\right\}. \tag{6}$$

In Eqn. 6, j indexes the number of ECS values for which we calculated $\overline{\lambda}_{c,sw,\tau_c}$, and the summation term on the right is the sum of the climate feedbacks from which the nominal $\overline{\lambda}_{c,sw,\tau_c}$ shown in Table 2 is subtracted. The difference between the summation term and the nominal $\overline{\lambda}_{c,sw,\tau_c}$ is equivalent to $1.36\,Wm^{-2}K^{-1}$. Each computed value of $(\overline{\lambda}_{c,sw,\tau_c})_j$ was added to the nominal contributions to SW cloud feedback due to changes in cloud amount and altitude (Table 3) to compute nine $(\overline{\lambda}_{c,sw})_j$ values – one for each ECS evaluated. This process was repeated for each partitioned SW and LW cloud feedback.

Finally, we estimated the relationship between each partitioned SW and LW Cloud Feedback and their corresponding cloud property trends. We used the monthly averaged 1° gridded CERES Edition 4 data products to estimate cloud radiative kernels by calculating the differences between select geophysical variables from July 2006 and July 2004 and using multiple linear regression to regress LW irradiance, SW irradiance over land, and SW irradiance over ocean on those variables. The data products acquired were the SW and LW TOA irradiance (flux), cloud fraction, cloud optical depth, cloud effective temperature, surface skin temperature, column-integrated wa-

ter vapor, and cloud emissivity. For consistency, we excluded regions poleward of 60° and snow or ice-covered non-polar regions in computing the July 2006 - July 2004 differences. The ocean and land SW irradiance was regressed onto cloud fraction and the relative $\log_{10}\tau_c$ (separated by land and ocean surface types with the USGS IGBP map). The LW irradiance was regressed onto cloud fraction, effective cloud top temperature, cloud emissivity, total column precipitable water, and surface skin temperature. The SW land and LW TOA irradiance anomalies computed with the multivariate linear regression results are each compared to their corresponding CERES-observed anomalies in Figure 3. The regression coefficients from multivariate linear regressions were used as the estimated radiative kernels (e.g. $\frac{\delta\%log_{10}(\tau)}{\delta F_{SW,ocean}}$) in these studies and are shown in Table 4.

We multiplied the cloud property-partitioned SW and LW cloud feedbacks by a global mean surface temperature trend of 0.25 K per decade to calculate TOA SW and LW irradiance trends (in $Wm^{-2}/decade$). Then, multiplying the radiative kernels and the SW and LW irradiance trends, we computed corresponding cloud property decadal trends. These analyses resulted in relationships among equilibrium climate sensitivity, cloud property trends (for cloud fraction, cloud effective temperature, and cloud optical thickness), and the SW and LW cloud feedback.

Similarly to Figure 2, Figure 4 shows the time to detect trends (Fig. 4a) and the delay compared to a perfect observing system in the time to detect trends (Fig. 4b) for reflected solar instruments with various calibration uncertainties in the 0.65 μm band. However, the Figure 4 optical thickness trend uncertainty range (left y-axis) has been adjusted using the additional information relating ECS and SW cloud feedback to optical thickness decadal trends and includes the AR5 ECS intermodel range shaded in gray. The farthest right y-axis shows the equivalent cloud optical thickness trend. The only difference between the left and farthest right y-axes is that the optical thickness trend has negative values, whereas trend uncertainty cannot be negative.

The resulting estimation of the relationship among ECS, SW cloud feedback, and cloud optical thickness trend uncertainty shows that the globally averaged optical thickness trend range falls between -0.56 %/decade (for 4.7 K ECS) and 0.39 %/decade (for 2.1 K ECS) (Fig. 4, shaded). With an instrument with a 0.65 μm absolute calibration accuracy of 0.3% (2σ) it would take 21–27 years to begin distinguishing trends from natural variability, depending on the magnitude of the trend, equivalent to a 2–4 year delay compared to a perfect instrument (i.e. one limited solely by natural variability). However, continuing with cloud imager absolute calibration levels comparable to those currently operational (e.g. 3.6%, 2σ), the trend detection delay compared to a perfect instrument is longer, between 60 and 76 years, depending upon the trend magnitude.

To evaluate the challenge of detecting a trend of smaller absolute magnitude in cloud optical thickness, which is possible, given the likely range of τ_c trends within the AR5 intermodel range, we turn to the nominal ECS that we calculated from our forcing-feedback calculation of 2.53 K. The corresponding estimated optical thickness trend is 0.1 %/decade, a trend closer to zero than those corresponding to a 2.1 K or 4.7 K ECS. It would take a perfect instrument 60 years to begin distinguishing this trend from natural variability, a feat that would take a CLARREO-like inter-calibration standard 66.7 years. With today's instrument accuracy requirements, we would wait over a century longer (187 years) before detecting this smaller trend. Figure 4 demonstrates that observations can most quickly eliminate large absolute trends in cloud optical depth, or equivalently, extreme values of climate sensitivity. The longer and more accurate the climate record, the tighter the constraint on ECS uncertainty.

The results related to the effective cloud temperature (T_e) trend, LW cloud feedback, and ECS are shown in Figure 5. We found a σ_{var} of 0.147 K and a κ_{var} of 0.679 years. Using the climate accuracy framework (Eqns. 4 and 5) with a sensitivity of cloud effective temperature to BT changes in the 11 μm band of 1.34 K/K, we determined that for a goal of 20% trend accuracy departure

from perfect, the 11 μm band requirement is 0.06 K (2σ), which is also the current CLARREO IR accuracy goal (W13). Applying our analysis to link the T_e trend, LW cloud feedback (upon which cloud temperature, and therefore altitude, has a greater impact than upon SW cloud feedback) and ECS, we estimate the range of T_e trends to be -0.036 K/decade (ECS of 2.1 K) to -0.33 K/decade (ECS of 4.7 K). This T_e trend range, illustrated in Fig. 6 by the shaded region, is predominantly negative, indicating rising cloud heights. This estimation is consistent with GCM simulations of cloud changes, their projections of a rising tropopause level, and their resulting calculations of positive LW cloud feedback due to rising cloud heights (Zelinka et al. 2012; Collins et al. 2013).

For the likely range of cloud effective temperature, the trend detection delay compared to a perfect instrument for a cloud imager inter-calibrated with a CLARREO-like spectrometer is 1 – 5 years. For today's instruments the delay would be longer, ranging between 21 – 95 years for a VIIRS-like calibration uncertainty of 0.54 K (2σ) and 26–117 years for a MODIS-like calibration uncertainty of 0.68 K (2σ).

For global cloud fraction, we found the σ_{var} to be 0.171 %, and the κ_{var} to be 1.35 years. For all instances of cloud fraction-related values, except in Table 1 where the relative σ_{var} and σ_{Vcal} are stated, cloud fraction is stated in percent cloud fraction ranging from 0% (clear)–100% (completely overcast). The CPRS cloud mask involves several MODIS bands, depending upon the scene. Among the four primary bands investigated in this study, the globally averaged cloud fraction exhibits the most sensitivity to the 11 and 12 μm bands. We determined globally averaged sensitivities of cloud fraction to BR changes in the 11 and 12 μm bands to be -0.28 and -0.35 %/K in the 11 and 12 μm bands, respectively. For these bands the 20%-from-perfect absolute calibration accuracy requirements are more more lenient than the 0.06 K CLARREO IR requirement at 0.47 K for the 11 μm band and 0.39 K for the 12 μm band. The impact of instrument calibration on the time to detect trends and the delay in detection time compared to a perfect in-

strument for both IR bands is shown in Figure 6. Note that the current VIIRS and MODIS absolute calibration uncertainties are less lenient than both 20%-from-perfect absolute calibration accuracy requirements.

These results for cloud fraction need to be considered with some caution, however. Recall that within these studies, we have thus far evaluated the sensitivity of cloud properties to changes in four MODIS bands independently, and we have determined the impact on time to detect trends in those cloud properties based on calibration requirements in each of those bands. This should not be the only way these requirements are evaluated, however, since within the CERES/MODIS cloud mask retrieval algorithm, bands may be used individually, such as the 11 μm band which is used to determine if the pixel is too cold to be cloud-free, or the combination of information between two bands may be used together, such as the difference between the BT in the 11 and 12 μm bands. Additionally several other cloud mask tests are often applied using reflectance and brightness temperature in different wavelengths depending on the cloud type encountered. For example, there are differences in determining thin high clouds versus low thick clouds.

We have conducted preliminary investigations that have demonstrated the impact of these cloud types differences on the sensitivity of cloud properties to changes in the four bands considered here. In these preliminary results, we have found that for different cloud types, the sensitivity of cloud fraction varies not only by magnitude but also by sign for the 11 μm band. Taking the 21-day cloud fraction-weighted average of these sensitivities gives the total cloud sensitivities used in the current study. The total cloud sensitivities used in this study, however, do not necessarily sufficiently represent the variability in the sensitivity among different cloud types. Further investigation, therefore, is required that also carefully examines the natural variability of the cloud properties of different cloud types, in addition to their RS and IR instrument calibration sensitivi-

ties, the combination of which would allow for determination of calibration requirements by cloud type.

b. Water Cloud Effective Radius

We also determined accuracy requirements for detecting trends in effective particle size of water clouds. In the CPRS, the effective particle radius, r_e, is retrieved primarily using the information about particle size in the 3.8 μm band. Using the method described above we determined the accuracy requirement for an instrument to provide sufficiently accurate data that would allow for trend detection within 20% from that of a perfect instrument, which we found to be 0.01 K. Although the current CLARREO design does not include the 3.8 μm band, this requirement is more stringent than the accuracy requirement for the CLARREO IR instrument (designed to span 5–50 μm). As in our previous analysis which quantified the relative trends in cloud properties in the context of the AR5 equilibrium climate sensitivity intermodel range, the 3.8 μm band requirements relative to water cloud effective radius must also be placed into a relevant context.

This climate change accuracy analysis for effective radius can be placed into a climate change-relevant context using the relationship between r_e and the aerosol indirect effect (Twomey 1977), or as it has more recently been named, the Effective Radiative Forcing due to aerosol-cloud interactions (ERFaci) (Stocker et al. 2013). Trends in the ERFaci can be linked to cloud changes in both cloud amount and optical depth (and, therefore, effective radius); however, in the following analysis, we focused solely on the connection between the ERFaci and optical depth. A decrease in water particle size, in a cloud with constant liquid water content, increases the total water droplet cross-sectional surface area, thus increasing the cloud optical depth. A decrease in water cloud effective particle size may indicate an increase in cloud condensation nuclei, which are typically

dominated by aerosol particles. We therefore evaluated the level of instrument accuracy required to detect trends in r_e to better constrain estimates of ERFaci.

Ultimately, we needed to estimate a relationship between aerosol forcing trends and effective radius trends. To quantify this relationship we used the 30 year forcing projections from the AR5 Representative Concentration Pathway 4.5 Wm^{-2} (RCP4.5) scenario (Collins et al. 2013). Between 2000 and 2030, the RCP4.5 total anthropogenic and natural Effective Radiative Forcing projected change is 1.31 Wm^{-2}. The total aerosol ERF (ERFari+aci) (Stocker et al. 2013), which includes aerosol cloud interactions (aci) and aerosol radiation interactions (ari) are nearly indistinguishable among the four RCPs, with the ERFari+aci becoming less negative by about 1 Wm^{-2} during the 21st century. Between 2000 (-1.17 Wm^{-2}) and 2030 (-0.91 Wm^{-2}) the ERFari+aci was projected to increase by 0.26 Wm^{-2}. However, to connect the aerosol ERF to the effective radius trend, we needed to isolate the ERFaci. AR5 radiative forcing estimates for 2011 relative to 1750 show that the ERFaci and ERFari contribute 50% each to the ERFaci+ari, each being about -0.45 Wm^{-2} (Myhre et al. 2013). Assuming this ratio remains approximately constant throughout the 21st century, we estimate an ERFaci change between 2000 and 2030 of 0.13 Wm^{-2} (0.043 Wm^{-2}/decade).

The ERFaci trend presented above ($\Delta ERFaci$) can be represented as

$$\Delta ERFaci = \Delta log_{10}(\tau_c)_w \frac{\partial CRE_{SW,w}}{\partial log_{10}(\tau_c)_w} \tag{7}$$

where the w subscript indicates water cloud, and $CRE_{SW,w}$ is the SW cloud radiative effect for water cloud. The radiative kernel, $\frac{\partial CRE_{SW,w}}{\partial log_{10}(\tau_c)_w}$ was computed in a manner similar to those described in the previous section and shown in Table 4, however, with minor differences. The previous radiative kernels were computed for the TOA SW and LW irradiance, whereas these were computed for the SW CRE. Additionally, because here the focus is on liquid water clouds, these kernels were

computed using one year of data to ensure a sufficient sample size. The resulting kernel value and its uncertainty is $\frac{\partial CRE_{SW,w}}{\partial log_{10}(\tau_c)_w} = -0.728 \pm 0.15\,\%/Wm^{-2}$. From Equation 7, we solve for the optical thickness trend, $\Delta log_{10}(\tau_c)_w$, and the relationship between this trend and an effective radius trend can be shown to be

$$\begin{aligned}\Delta log_{10}(\overline{\tau_c}) &= \Delta log_{10}\Big\{C\frac{\overline{LWP}}{\overline{r_e}}\Big\} \\ &= \Delta log_{10}(C) + \Delta log_{10}(\overline{LWP}) - \Delta log_{10}(\overline{r_e}) \qquad (8)\end{aligned}$$

$$\Delta log_{10}(\overline{\tau_c}) = -\Delta log_{10}(\overline{r_e}) \qquad (9)$$

From Slingo (1989), we use the parameterization that approximates the relationship between water cloud τ_c and r_e, where C is a constant approximated by $h * 3/2$, with h being the geometric cloud height, and $\overline{LWP}$ is the globally averaged liquid water path. Equation 8 simplifies to Equation 9, considering logarithm rules and that both C and LWP are constants, so the trends of their logarithms are zero. Combining Equations 9 and 7 provides a relationship between the ERFaci and the ($\log_{10}$) water cloud effective radius. In addition to the AR5 projected change of the total ERF, we modified the ERFaci to cover a range of values and computed the corresponding water cloud effective radius trend (relative trend of the base-10 logarithm of the effective radius). This relationship and the expanded analysis covering a range of potential ERFaci trends linked to corresponding r_e trends is shown in Figure 7.

For the specific AR5 projection discussed above for which the ERFaci trend was 0.043 Wm^{-2}/decade, the corresponding relative $log_{10}r_e$ trend is 0.06 %/decade. It would take a perfect instrument 19 years to detect this trend. For an instrument capable of detecting trends within an uncertainty of 20% from perfect (0.01 K, 2σ) the delay beyond a perfect instrument would be 1.5 years. With a CLARREO-like instrument, the delay would be 22 years. For instruments

comparable to today's operational IR cloud imagers, the delay in trend detection time would be over a century.

These results need to be considered with care, as we have made several assumptions within this analysis, which we have included in our description above; however, despite the idealized context within which we obtained these results, our analysis provides important information regarding the impact of calibration requirements on quantifying the aerosol indirect effect, which is among the greatest uncertainties in radiative forcing. We have shown that with an instrument with a comparable absolute calibration requirement to the CLARREO IR spectrometer, trends in effective radius, and therefore ERFaci could be detected at about eight or nine decades sooner than with existing instruments. These results illustrate, similarly to the results from W13, the importance of stringent accuracy requirements for climate change trend detection. This study was conducted solely using the effective radius retrieved using the 3.8 μm band; however, it would also be relevant to extend this study to investigate the impact of absolute calibration accuracy on the time to detect trends in water cloud effective radius retrieved using reflectance in the 1.6 μm and 2.1 μm bands.

5. Summary, Discussion, and Conclusions

Reducing cloud property trend detection times and trend uncertainties using measurements from instruments with sufficiently high accuracies for climate change detection and attribution would contribute significantly to improved understanding of climate processes. In these studies we applied a climate accuracy framework (Wielicki et al. 2013) (W13) to enable quantitatively-based justification for determining what constitutes *sufficient accuracy requirements* for timely cloud property trend detection. We applied this climate accuracy framework to quantify the impact of absolute calibration accuracy of reflected solar and infrared instruments on the trend detection time of cloud properties retrieved by the CERES/MODIS Cloud Property Retrieval System (Wielicki

et al. 1996; Minnis et al. 2011). Our results demonstrate a quantitative basis upon which to determine climate accuracy requirements to detect changes in cloud properties and understand their relationships to changes in Earth's climate system.

In our studies, we followed the CLARREO goal for detection of climate variable trends at no more than 20% degradation relative to the accuracy of a perfect observing system. With these goals, the absolute calibration requirements determined using cloud radiative effect and global mean surface temperature were 0.3% for the reflected solar spectrometer and 0.06 K for the infrared spectrometer, respectively (W13). However, until the current study no other similar goals had been formally evaluated for other essential climate variables, such as cloud properties. Here, we focused on four cloud properties: cloud fraction, cloud optical thickness, cloud effective temperature, and effective radius.

To quantify the impact of different instrument absolute accuracy requirements for clarifying climate change impacts and relationships, we also estimated relationships among trends in cloud properties (cloud fraction, optical thickness, and effective temperature), equilibrium climate sensitivity, and SW and LW cloud feedback. This analysis provides a quantitive context within which necessary and sufficient accuracy requirements can be defined for future climate change observing instruments and to reduce uncertainty in ECS, which is dominated by uncertainty in cloud feedback. Linking these quantities provides an estimation of the potential cloud property trend magnitudes that could be expected for a range of climate sensitivities and SW and LW cloud feedbacks. Additionally, this analysis quantifies the differences in cloud property trend detection time considering RS and IR instruments with various absolute calibration uncertainties.

The CLARREO RS requirement of 0.3% (2σ) is nearly equivalent to the requirement for an instrument detecting cloud optical thickness trends with a 20% degradation relative to a perfect instrument in the 0.65 μm band, which we found to be 0.27%. In linking cloud optical thickness

trends to the SW cloud feedback and ECS, we found that relative $log_{10}\tau_c$ trends are likely to fall between -0.56 %/decade and 0.39 %/decade for Equilibrium Climate Sensitivities of 4.7 K and 2.1 K, respectively. For an ECS of 2.53 K (our nominal ECS determined from the forcing-feedback framework), we estimated a cloud optical thickness trend of 0.1 %/decade. The delay compared to a perfect observing system in detecting trends within the AR5 ECS intermodel range spanned about 2–7 years for a CLARREO-like instrument to several decades for instruments with accuracy requirements comparable to that of today's instruments (60 years to more than a century).

The climate accuracy framework applied to cloud effective temperature revealed a 0.06 K requirement for the 11 μm band for an instrument with a 20% degradation compared to a perfect instrument, which is equivalent to the current CLARREO IR requirement of 0.06 K (2σ). Because cloud altitude (for which cloud effective temperature is a proxy) has a stronger impact on LW than SW cloud feedback, we linked trends in cloud effective temperature, LW cloud feedback, and ECS. This revealed that for the AR5 ECS intermodel range, the effective temperature trend may fall between -0.036 K/decade and -0.33 K/decade for ECS values between 2.1 K and 4.7 K, respectively. Detection times for instruments with calibration requirements similar to today's instruments (0.54 K–0.68 K) spans 20 years to more than a century. For a CLARREO-like IR instrument, detection delays are shorter, between 1 and 5 years, illustrating the benefit of highly accurate climate sensors. The IR requirements that we determined for detecting trends in cloud effective temperature at a 20% from perfect degradation (comparable to CLARREO) would provide a substantial improvement in detection time compared to continuing with the absolute calibration accuracy of currently operational IR sensors.

To detect trends in cloud fraction using the goal of detecting trends with trend uncertainties that are 20% from those detected by a perfect instrument, the 11 and 12 μm band requirements are 0.47 K and 0.39 K (2σ). These requirements are less stringent than the current CLARREO

design of 0.06 K (2σ) but more stringent compared to today's cloud imager absolute accuracies. A more rigorous analysis of cloud fraction by cloud type is required to determine cloud fraction-driven climate accuracy requirements, given the complex dependence of the CPRS cloud mask for different cloud types on multiple MODIS bands. Our analyses provide the first direct link between satellite instrument calibration requirements and their impact on constraints on ECS and the detection time of climate change-scale cloud property trends.

For detecting trends in water cloud effective radius (r_e), we determined that a 20%-from-perfect requirement is much more stringent than the current CLARREO IR accuracy requirement and is close to perfect at 0.01 K (2σ). To extend our analysis to climate process variables, we linked trends in r_e to Effective Radiative Forcing due to aerosol cloud interactions (ERFaci) using the aerosol indirect effect mechanism. We used information from AR5 projections to find that detection times of r_e could be reduced by about eight decades with a CLARREO-like instrument calibration requirement compared to today's instruments.

Further studies to evaluate other essential climate variables with quantitative frameworks such as that presented by W13 and demonstrated here will become increasingly important within the current US and global challenge to appropriate sufficient resources for climate change monitoring. With the challenge of limited Earth Science funding to develop high-accuracy instruments for climate change detection and attribution, using quantitative studies such as these can provide more rigorous justification for the design of new climate change satellite, aircraft-based, surface, and in-situ sensors. A similar method for determining the required quality of climate change measurements has been demonstrated in the report on *Continuity of NASA Earth Observations from Space* (National Research Council 2015), illustrating the increasing importance of conducting such studies on a more extensive range of essential climate variables to provide the climate community with a more quantitative understanding of climate change measurement requirements.

This study demonstrates the value of applying the climate accuracy framework and techniques for placing the results from that framework application into a climate change-relevant context. As these studies are continued, various implementation details can be revised to further refine the utility and meaning of these results. Although we focused on trends in individual cloud properties and connected the value of improving trend detection time to climate model projections, applying cloud fingerprints may help to detect secular trends more rapidly (e.g. Marvel et al. (2015); Roberts et al. (2014); Jin and Sun (2016)). In this study, we limited our analysis to evaluating the impact of calibration requirements in individual bands on trend detection times; however, evaluating cloud property trend detection impacts of calibration requirements in multiple instrument bands simultaneously would provide a more realistic analysis. Because the CERES CPRS was used to quantify the sensitivity of cloud properties to gain and offset changes in MODIS data, the results from our study are dependent upon the retrieval algorithm used; therefore, it would also be valuable to extend these studies to other cloud imagers (e.g. VIIRS) and algorithms (e.g. MODIS-ST).

In these studies, we focused on global trends in cloud properties for total cloud, without regard for regional or individual cloud type contributions; however, climate projections have indicated that different cloud types on both a global and regional scale respond differently to and exert different feedbacks upon Earth's changing climate. For example, there is a need for better constraint of low cloud processes to reduce uncertainty of the low cloud SW feedback and, ultimately, equilibrium climate sensitivity. It would be valuable, therefore, to expand the results of these studies to two-dimensional cloud type histograms. These analyses could then be expanded to link instrument requirements and their impact on cloud trend detection to climate model projections for those different cloud types, which would help to provide more specific constraints regarding instrument requirements.

To estimate the natural variability of cloud properties here, we used data from operational satellites (CERES/MODIS cloud properties), combined with statistical adjustments to account for the short annual time series and any potential secular linear trends. This, of course, assumes that the anomalies in cloud properties measured from satellite adequately represent cloud property natural variability.

Our ability to detect cloud property trends is limited by the natural variability and instrument accuracy, as we have investigated in these studies, but trend detection uncertainty is also dependent upon uncertainties in inferring cloud properties from satellite measurements. Large climate change scale uncertainties in retrieval algorithms could be erroneously identified as secular geophysical changes in the climate system or could mask or distort the true physically-driven climate change trends occurring in the climate system. In addition to evaluating the impact of instrument uncertainty on trend detection, the impact of time-invariable biases and uncertainties in geophysical retrieval algorithms on trend detection accuracy in cloud properties and other essential climate variables must also be quantified, and, if possible reduced.

Acknowledgments. The authors would like to thank David Doelling for his help with obtaining the CERES Edition 4A Cloud Property Data. P. Minnis and S. Sun-Mack are supported by the CERES Program. Y. Shea and B. Wielicki are supported by CLARREO Pre-formulation funding.

References

Chen, T., W. B. Rossow, and Y. Zhang, 2000: Radiative effects of cloud-type variations. *Journal of Climate*, **13 (1)**.

Collins, M., and Coauthors, 2013: *Long-term Climate Change: Projections, Commitments and Irreversibility. In: Climate Change 2013: The Physical Science Basis. Contribution of Working*

Group I to the Fifth Assessment Report of the Intergovernmental Panel on Climate Change, book section 12, 1029–1136. Cambridge University Press, Cambridge, United Kingdom and New York, NY, USA, doi:10.1017/CBO9781107415324.024, URL www.climatechange2013.org.

Dolinar, E. K., X. Dong, B. Xi, J. H. Jiang, and H. Su, 2014: Evaluation of CMIP5 simulated clouds and TOA radiation budgets using NASA satellite observations. *Climate Dynamics*, **44 (7-8)**, 2229–2247.

Feldman, D. R., C. A. Algieri, W. D. Collins, Y. L. Roberts, and P. A. Pilewskie, 2011: Simulation studies for the detection of changes in broadband albedo and shortwave nadir reflectance spectra under a climate change scenario. *Journal of Geophysical Research: Atmospheres (1984–2012)*, **116 (D24)**.

Flato, G., and Coauthors, 2013: *Evaluation of Climate Models. In: Climate Change 2013: The Physical Science Basis. Contribution of Working Group I to the Fifth Assessment Report of the Intergovernmental Panel on Climate Change*, book section 9, 741–866. Cambridge University Press, Cambridge, United Kingdom and New York, NY, USA, doi:10.1017/CBO9781107415324.020.

Jin, Z., and M. Sun, 2016: An initial study on climate change fingerprinting using the reflected solar spectra. *Journal of Climate*, **29 (8)**, 2781–2796, doi:10.1175/JCLI-D-15-0297.1.

Kato, S., F. G. Rose, X. Liu, B. A. Wielicki, and M. G. Mlynczak, 2014: Retrieval of atmospheric and cloud property anomalies and their trend from temporally and spatially averaged infrared spectra observed from space. *Journal of Climate*, **27 (12)**, 4403–4420.

Leroy, S. S., J. G. Anderson, and G. Ohring, 2008: Climate signal detection times and constraints on climate benchmark accuracy requirements. *Journal of Climate*, **21 (4)**, 841–846.

Loeb, N. G., J. M. Lyman, G. C. Johnson, R. P. Allan, D. R. Doelling, T. Wong, B. J. Soden, and G. L. Stephens, 2012: Observed changes in top-of-the-atmosphere radiation and upper-ocean heating consistent within uncertainty. *Nature Geoscience*, **5 (2)**, 110–113.

Loeb, N. G., B. A. Wielicki, D. R. Doelling, G. L. Smith, D. F. Keyes, S. Kato, N. Manalo-Smith, and T. Wong, 2009: Toward optimal closure of the earth's top-of-atmosphere radiation budget. *Journal of Climate*, **22 (3)**, 748–766.

Loveland, T., B. Reed, J. Brown, D. Ohlen, Z. Zhu, L. Yang, and J. Merchant, 2000: Development of a global land cover characteristics database and IGBP DISCover from 1 km AVHRR data. *International Journal of Remote Sensing*, **21 (6-7)**, 1303–1330.

Lyapustin, A., and Coauthors, 2014: Scientific impact of MODIS C5 calibration degradation and C6+ improvements. *Atmospheric Measurement Techniques*, **7 (12)**, 4353–4365, doi:10.5194/amt-7-4353-2014.

Marvel, K., M. Zelinka, S. A. Klein, C. Bonfils, P. Caldwell, C. Doutriaux, B. D. Santer, and K. E. Taylor, 2015: External influences on modeled and observed cloud trends. *Journal of Climate*, **28 (12)**, 4820–4840.

Minnis, P., and Coauthors, 2008: Cloud detection in nonpolar regions for CERES using TRMM VIRS and Terra and Aqua MODIS data. *Geoscience and Remote Sensing, IEEE Transactions on*, **46 (11)**, 3857–3884.

Minnis, P., and Coauthors, 2011: CERES edition-2 cloud property retrievals using TRMM VIRS and Terra and Aqua MODIS data Part I: Algorithms. *Geoscience and Remote Sensing, IEEE Transactions on*, **49 (11)**, 4374–4400.

Myhre, G., and Coauthors, 2013: *Anthropogenic and Natural Radiative Forcing. In: Climate Change 2013: The Physical Science Basis. Contribution of Working Group I to the Fifth Assessment Report of the Intergovernmental Panel on Climate Change*, book section 8, 659740. Cambridge University Press, Cambridge, United Kingdom and New York, NY, USA, doi: 10.1017/CBO9781107415324.018, URL www.climatechange2013.org.

National Research Council, 2007: *Earth Science and Applications from Space: National Imperatives for the Next Decade and Beyond*. National Academy Press, 428 pp.

National Research Council, 2015: *Continuity of NASA Earth Observations from Space: A Value Framework*. National Academies Press.

Nolin, A., R. L. Armstrong, and J. Maslanik, 1998: Near-real-time SSM/I-SSMIS EASE-Grid daily global ice concentration and snow extent. Boulder, Colorado USA: National Snow and Ice Data Center. *Digital media. Updated daily*.

Ohring, G., B. Wielicki, R. Spencer, B. Emery, and R. Datla, 2005: Satellite instrument calibration for measuring global climate change: Report of a workshop. *Bulletin of the American Meteorological Society*, **86 (9)**.

Phojanamongkolkij, N., S. Kato, B. A. Wielicki, P. C. Taylor, and M. G. Mlynczak, 2014: A comparison of climate signal trend detection uncertainty analysis methods. *Journal of Climate*, **27 (9)**, 3363–3376.

Roberts, Y., P. Pilewskie, D. Feldman, B. Kindel, and W. Collins, 2014: Temporal variability of observed and simulated hyperspectral reflectance. *Journal of Geophysical Research: Atmospheres*, **119 (17)**, 10–262.

Roithmayr, C., C. Lukashin, P. Speth, D. Young, B. Wielicki, K. Thome, and G. Kopp, 2014a: Opportunities to intercalibrate radiometric sensors from International Space Station. *Journal of Atmospheric and Oceanic Technology*, **31 (4)**, 890–902.

Roithmayr, C. M., C. Lukashin, P. W. Speth, G. Kopp, K. Thome, B. Wielicki, D. F. Young, and Coauthors, 2014b: CLARREO approach for reference intercalibration of reflected solar sensors: On-orbit data matching and sampling. *Geoscience and Remote Sensing, IEEE Transactions on*, **52 (10)**, 6762–6774.

Roman, J., R. Knuteson, and S. Ackerman, 2014: Time-to-detect trends in precipitable water vapor with varying measurement error. *Journal of Climate*, **27 (21)**, 8259–8275.

Slingo, A., 1989: A GCM parameterization for the shortwave radiative properties of water clouds. *Journal of the Atmospheric Sciences*, **46 (10)**, 1419–1427.

Stephens, G. L., 2005: Cloud feedbacks in the climate system: A critical review. *Journal of climate*, **18 (2)**.

Stephens, G. L., S.-C. Tsay, P. W. Stackhouse Jr, and P. J. Flatau, 1990: The relevance of the microphysical and radiative properties of cirrus clouds to climate and climatic feedback. *Journal of the atmospheric sciences*, **47 (14)**, 1742–1754.

Stocker, T. F., and Coauthors, 2013: Climate change 2013: The physical science basis. *Intergovernmental Panel on Climate Change, Working Group I Contribution to the IPCC Fifth Assessment Report (AR5)(Cambridge Univ Press, New York)*.

Taylor, K. E., R. J. Stouffer, and G. A. Meehl, 2012: An overview of CMIP5 and the experiment design. *Bulletin of the American Meteorological Society*, **93 (4)**, 485–498.

Trepte, Q., P. Minnis, and R. F. Arduini, 2003: Daytime and nighttime polar cloud and snow identification using MODIS data. *Third International Asia-Pacific Environmental Remote Sensing Remote Sensing of the Atmosphere, Ocean, Environment, and Space*, International Society for Optics and Photonics, 449–459.

Twomey, S., 1977: The influence of pollution on the shortwave albedo of clouds. *Journal of the atmospheric sciences*, **34 (7)**, 1149–1152.

Weatherhead, E. C., and Coauthors, 1998: Factors affecting the detection of trends: Statistical considerations and applications to environmental data. *Journal of Geophysical Research: Atmospheres (1984–2012)*, **103 (D14)**, 17 149–17 161.

Wielicki, B. A., B. R. Barkstrom, E. F. Harrison, R. B. Lee III, G. Louis Smith, and J. E. Cooper, 1996: Clouds and the Earth's radiant energy system (CERES): An earth observing system experiment. *Bulletin of the American Meteorological Society*, **77 (5)**, 853–868, doi: 10.1175/1520-0477.

Wielicki, B. A., and Coauthors, 2013: Achieving climate change absolute accuracy in orbit. *B. Am. Meteorol. Soc.*

Zelinka, M. D., S. A. Klein, and D. L. Hartmann, 2012: Computing and partitioning cloud feedbacks using cloud property histograms. Part II: Attribution to changes in cloud amount, altitude, and optical depth. *Journal of Climate*, **25 (11)**, 3736–3754.

Zelinka, M. D., S. A. Klein, K. E. Taylor, T. Andrews, M. J. Webb, J. M. Gregory, and P. M. Forster, 2013: Contributions of different cloud types to feedbacks and rapid adjustments in cmip5. *Journal of Climate*, **26 (14)**, 5007–5027.

LIST OF TABLES

TABLE 1. Natural variability parameters calculated for the following cloud properties: Cloud Fraction (0-100%), $\log_{10}$ optical thickness (τ_c), Effective Temperature (T_c), and Liquid Water Effective Radius (r_e). Relative standard deviations were calculated relative to the 2002–2013 CERES/MODIS Aqua global mean and multiplied by 100%.

	Mean	κ_{var}[Years]	σ_{var}	σ_{var} (Rel.)	σ_{Vcal}	σ_{Vcal} (Rel.)
Cloud Fraction	66.3%	1.35	0.171%	0.258%	0.0591%	0.0889%
$\text{Log}_{10}(\tau_c)$	0.610	0.850	0.00379	0.621%	0.00104	0.170%
T_e	262 K	0.679	0.147 K	0.0560%	0.0359 K	0.0137%
$\text{Log}_{10}(r_e)$ (Liquid)	1.15 μm	0.753	8.59 x 10^{-4} μm	0.0748%	2.21 x 10^{-4}	0.0193%

TABLE 2. Partial derivatives (sensitivities) are given that represent the absolute (relative) sensitivity of cloud properties to offset (gain) changes in brightness temperature (reflectance). Sensitivity uncertainties were computed using the standard deviations of the global daily averages.

	$\frac{\partial log_{10}(\tau_c)}{\partial R_{0.65\mu m}}$ [$^{\%}/_{\%}$]	$\frac{\partial CF(\%)}{\partial BT_{11\mu m}}$ [$^{\%}/_{K}$]	$\frac{\partial CF(\%)}{\partial BT_{12\mu m}}$ [$^{\%}/_{K}$]	$\frac{\partial T_e}{\partial BT_{11\mu m}}$ [$^{K}/_{K}$]	$\frac{\partial log_{10}(r_e)}{\partial BT_{3.8\mu m}}$ [$^{\mu m}/_{K}$]
Average Sensitivity	1.38	-0.28	-0.35	1.34	-0.0370
2σ Sensitivity Uncertainty	$\pm$ 0.0282	$\pm$ 1.25 x 10^{-3}	$\pm$ 1.19 x 10^{-3}	$\pm$ 0.0620	$\pm$ 1.14 x 10^{-3}

TABLE 3. The non-cloud feedbacks used are the ensemble averages from the IPCC AR5 doubled CO_2 model runs. The SW and LW cloud property-partitioned cloud feedbacks are those calculated by Zelinka et al. (2013) from abrupt quadrupled CO_2 model runs, neglecting rapid adjustments, using CFMIP2/CMIP5 model output.

2 X CO_2 Radiative Forcing ($\overline{RF}$)	$3.7\,Wm^{-2}$		
Planck Feedback ($\overline{\lambda}_0$)	$-3.2\,Wm^{-2}K^{-1}$		
Water Vapor Feedback ($\overline{\lambda}_w$)	$1.6\,Wm^{-2}K^{-1}$		
Surface Albedo Feedback ($\overline{\lambda}_a$)	$0.3\,Wm^{-2}K^{-1}$		
Lapse Rate Feedback ($\overline{\lambda}_L$)	$-0.6\,Wm^{-2}K^{-1}$		
SW Cloud Feedback ($\overline{\lambda}_{c,sw}$)	$0.16\,Wm^{-2}K^{-1}$	Partitioned SW CF Contributions	
		Cloud Fraction ($\overline{\lambda}_{c,sw,frac}$)	$0.33\,Wm^{-2}K^{-1}$
		Cloud Altitude ($\overline{\lambda}_{c,sw,h}$)	$-0.07\,Wm^{-2}K^{-1}$
		Cloud Optical Depth ($\overline{\lambda}_{c,sw,\tau}$)	$-0.10\,Wm^{-2}K^{-1}$
LW Cloud Feedback ($\overline{\lambda}_{c,lw}$)	$0.28\,Wm^{-2}K^{-1}$	Partitioned LW CF Contributions	
		Cloud Fraction ($\overline{\lambda}_{c,lw,frac}$)	$-0.17\,Wm^{-2}K^{-1}$
		Cloud Altitude ($\overline{\lambda}_{c,lw,h}$)	$0.42\,Wm^{-2}K^{-1}$
		Cloud Optical Depth ($\overline{\lambda}_{c,lw,\tau}$)	$0.03\,Wm^{-2}K^{-1}$

804 TABLE 4. Multiple linear regression coefficients and their 1σ uncertainties. The coefficients are computed
805 from CERES observations and are used as radiative kernels.

Coefficient	SW Land Regression	SW Ocean Regression	LW Regression
$\frac{\partial \%log_{10}\tau_c}{\partial F_{SW}}$	0.261 $\pm$ 2.90 x 10^{-3}	0.256 $\pm$ 1.80 x 10^{-3}	
$\frac{\partial CF}{\partial F_{SWorLW}}$	0.805 $\pm$ 7.78 x 10^{-3}	0.757 $\pm$ 5.58 x 10^{-3}	-0.325 $\pm$ 3.97 x 104^{-3}
$\frac{\partial T_c}{\partial F_{LW}}$			0.825 $\pm$ 4.96 x 10^{-3}
$\frac{\partial \varepsilon}{\partial F_{LW}}$			-41.7 $\pm$ 0.524
$\frac{\partial WV}{\partial F_{LW}}$			-5.93 $\pm$ 0.106
$\frac{\partial T_s}{\partial F_{LW}}$			-0.929 $\pm$ 3.16 x 10^{-2}

LIST OF FIGURES

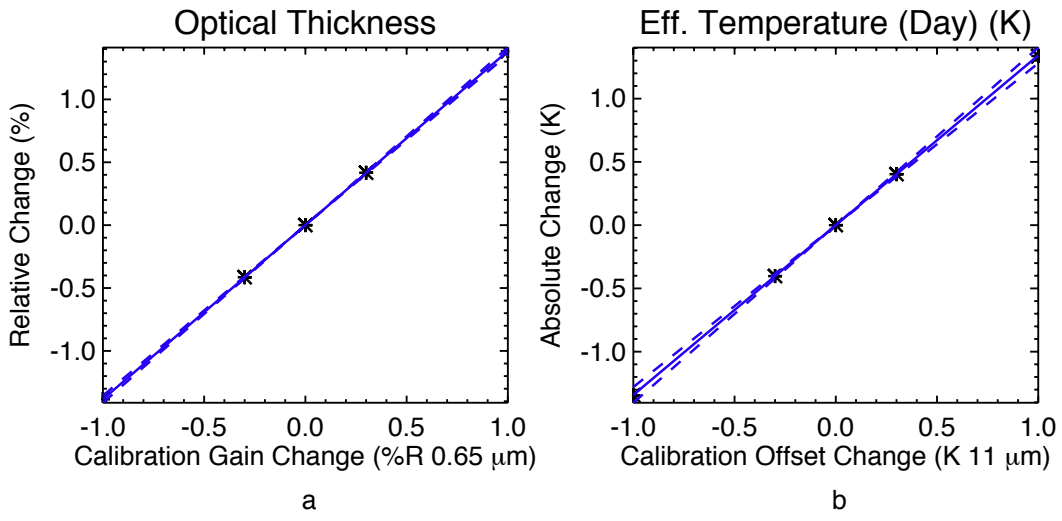

FIG. 1. The slope of the solid line shown in (a) provides the relative sensitivity of the $\log_{10}$ cloud optical depth ($\log_{10}\tau_c$) to gain calibration changes in the 0.65 μm MODIS reflectance. The slope of the solid line in (b) provides the sensitivity of the cloud effective temperature to offset calibration changes in the 11 μm MODIS brightness temperature. The uncertainty in sensitivity (uncertainty in slope) is shown by the two dashed lines in each figure. The four data points (excluding the origin point) are the global, 21-day averages of the CPRS-retrieved cloud property change due to a change in instrument calibration.

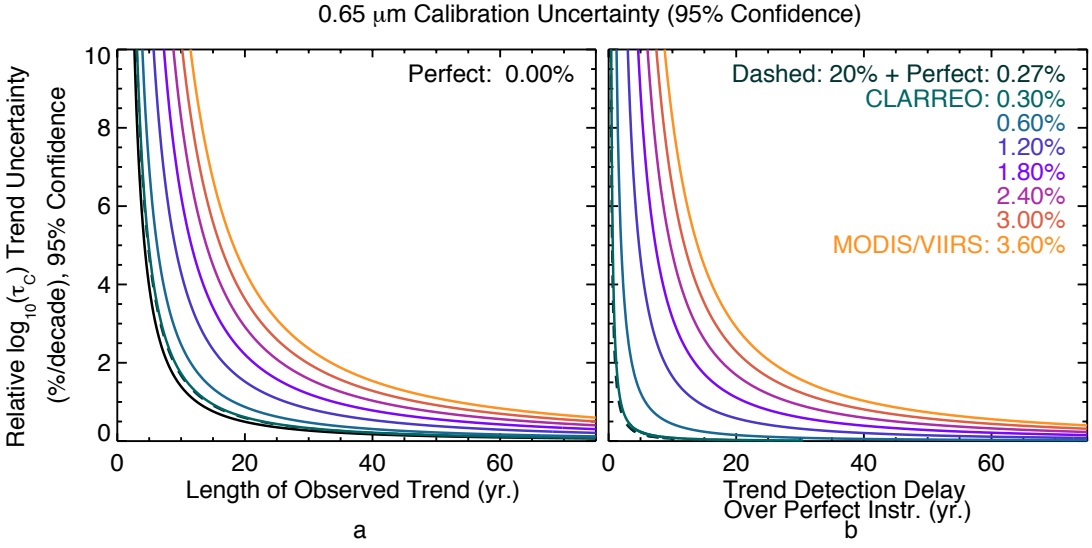

FIG. 2. For a range of 0.65 μm band 2σ calibration uncertainties, the 2σ cloud optical thickness trend uncertainty in relative $\log_{10}\tau_c$ (%) per decade is shown versus a) trend detection time and b) the delay in the detection time compared to a perfect observing system. The dashed line shows the requirement determined for an instrument capable of detecting trends within 20% trend uncertainty compared to a perfect observing system.

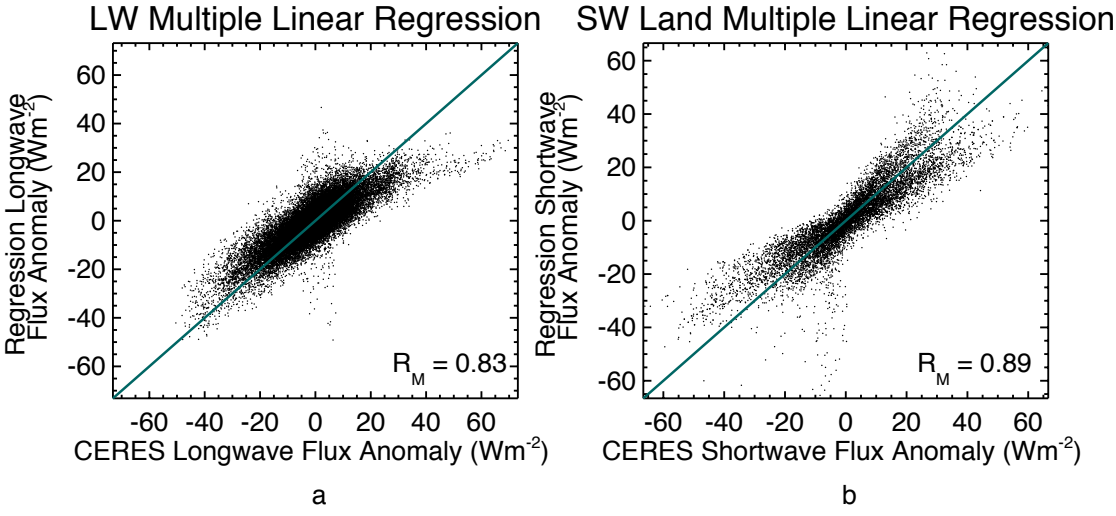

FIG. 3. The CERES TOA irradiance (flux) anomaly differences between July 2004 and July 2006 from the a) LW and b) SW land multiple linear regressions are compared to the CERES TOA LW and SW land irradiance anomaly differences in a) and b), respectively. The multivariate regression (R_M) coefficients for each regression are also shown. Although not shown, the SW Ocean comparison is similar to that of the land, as seen by the similarity of regression coefficients in Table 4.

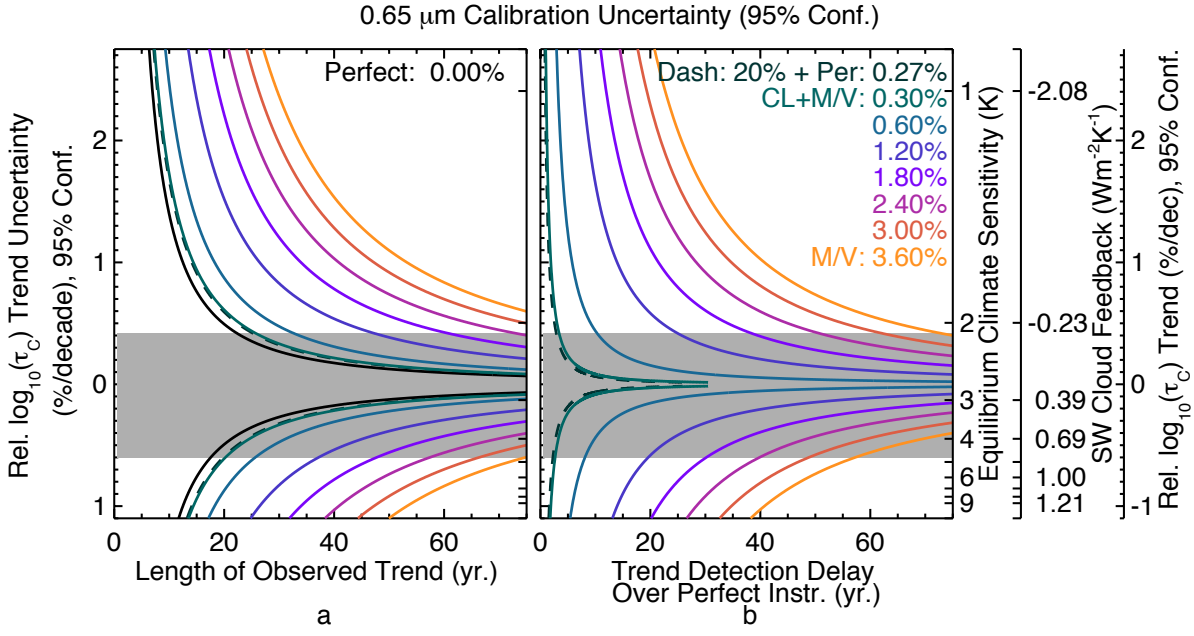

871 FIG. 4. Same as Figure 2, except the optical thickness trend uncertainty (left y-axis) and trend (far right y-axis)
872 are shown linked with the Equilibrium Climate Sensitivity (ECS) (K) and SW Cloud Feedback ($Wm^{-2}K^{-1}$)
873 (right y-axes). The gray shaded region shows the AR5 intermodel ECS range (2.1 K – 4.7 K). *CL+M/V*
874 denotes current CLARREO RS 2σ absolute calibration requirement. *M/V* denotes the approximate current
875 MODIS/VIIRS absolute 2σ calibration uncertainty.

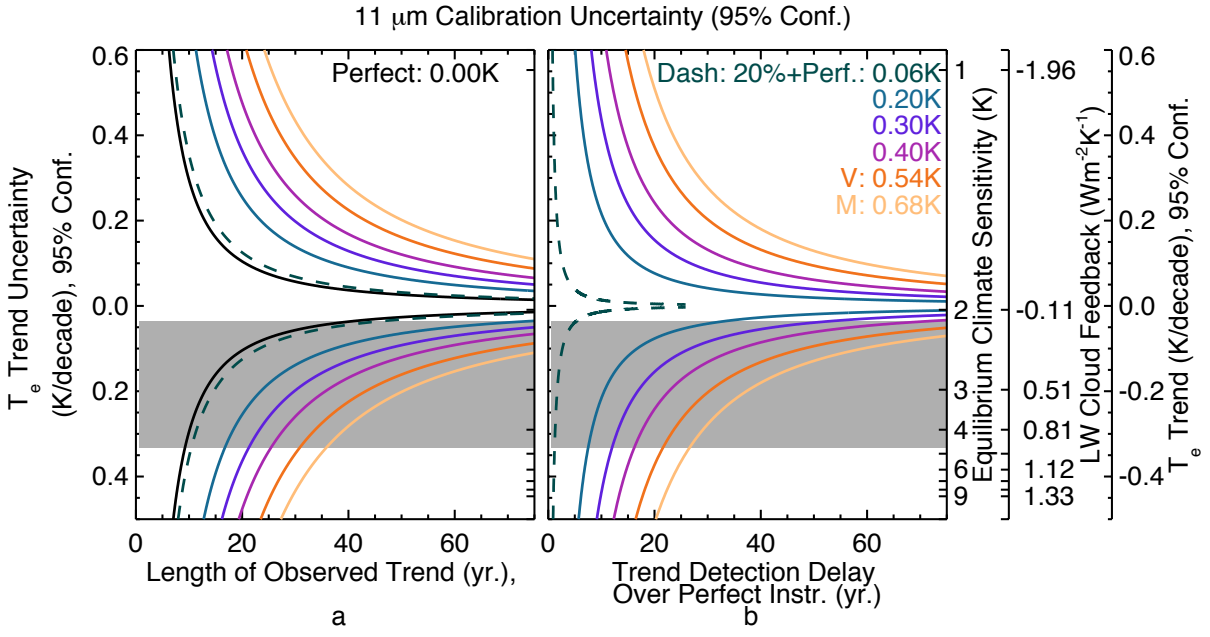

FIG. 5. For a range of 11 μm absolute calibration uncertainties, the time to detect trends (a) and the delay in detecting trends in cloud effective temperature (K/decade) with a real instrument compared to a perfect instrument (b) are shown linked with the Equilibrium Climate Sensitivity (ECS) (K) and LW Cloud Feedback ($\mathrm{Wm^{-2}K^{-1}}$). The gray shaded region shows the AR5 intermodel ECS range (2.1 K – 4.7 K). The dashed line shows the requirement determined for an instrument capable of detecting trends within 20% trend uncertainty compared to a perfect observing system. *V* and *M* denote the absolute calibration accuracies in the 11 μm bands for VIIRS and MODIS, respectively.

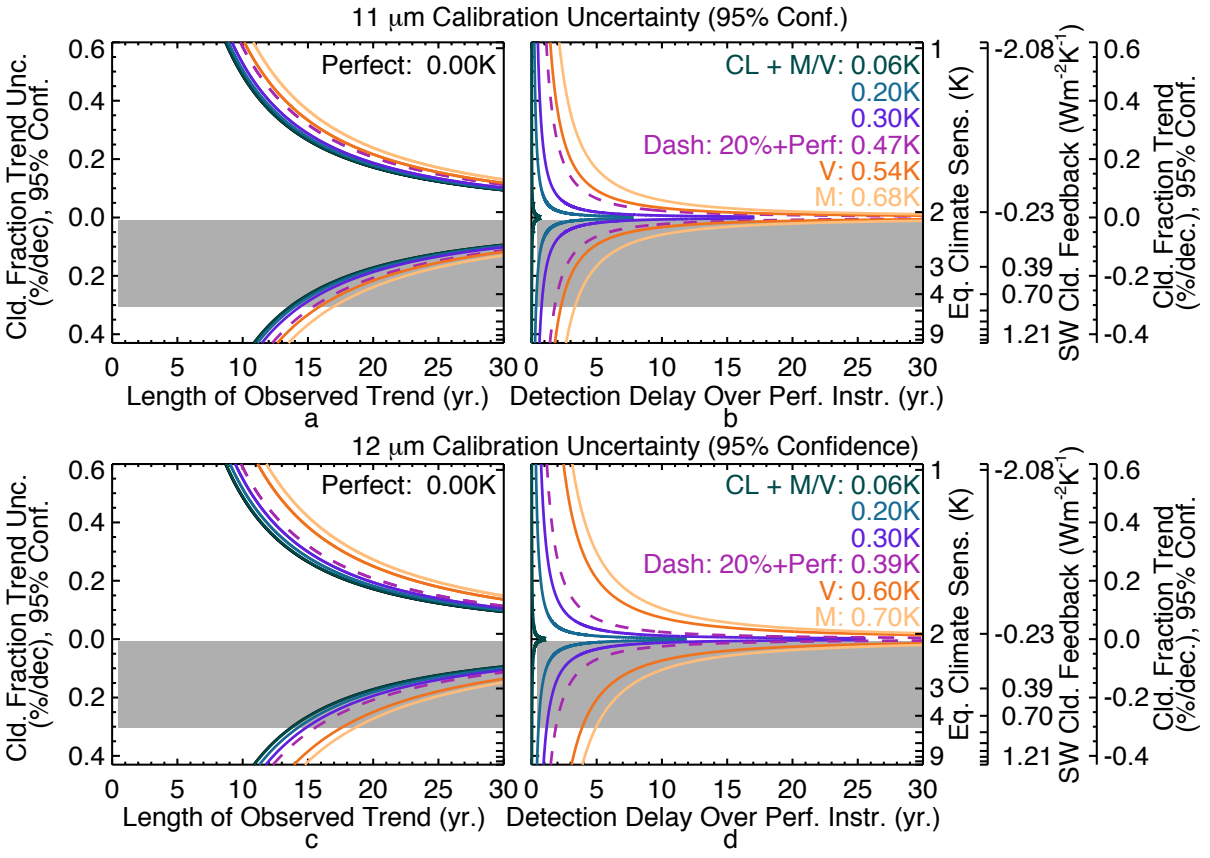

FIG. 6. For a range of 11 μm (top) and 12 μm (bottom) 2σ absolute calibration uncertainties the time to detect trends (left) and delay in detecting trends in cloud fraction (%/decade) (right) with a real instrument compared to a perfect instrument are shown linked with Equilibrium Climate Sensitivity (ECS) (K) and SW Cloud Feedback ($\mathrm{Wm^{-2}K^{-1}}$). The gray shaded region on the figure shows the AR5 intermodel ECS range (2.1 K – 4.7 K). The dashed line shows the requirement determined for an instrument capable of detecting trends within 20% trend uncertainty compared to a perfect observing system. *CL+M/V* denotes current CLARREO RS 2σ absolute calibration requirement. *V* and *M* denote the absolute calibration accuracies in the 11 μm and 12 μm bands for VIIRS and MODIS, respectively.

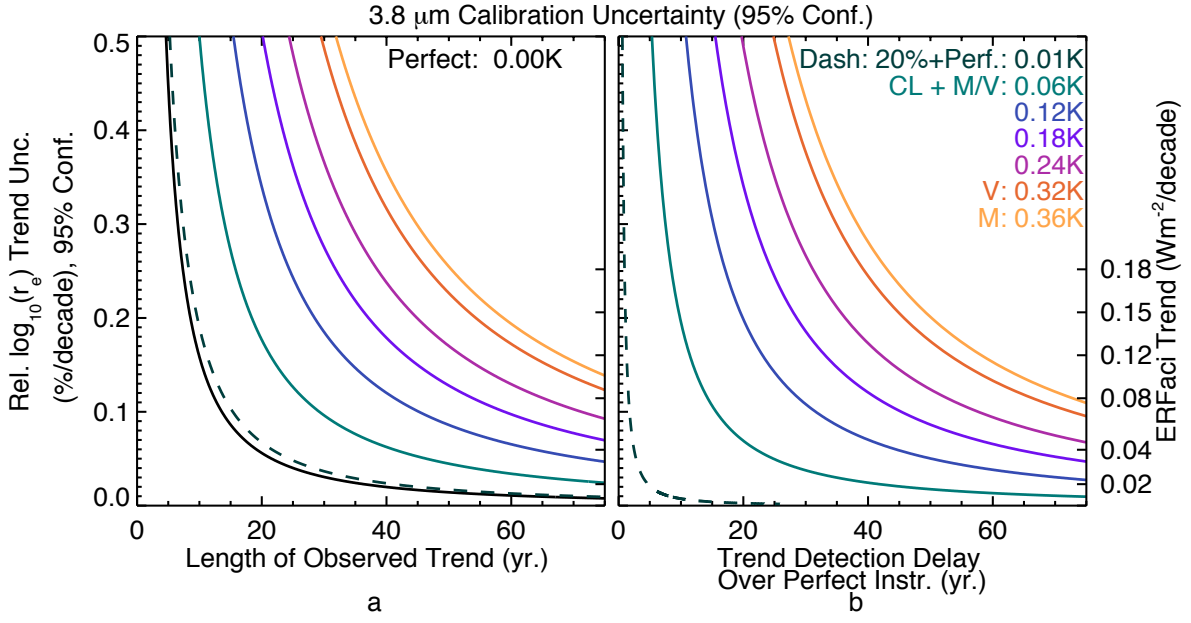

FIG. 7. For a range of 3.8 μm 2σ absolute calibration uncertainties the time to detect trends (left) and delay in detecting trends in water cloud effective radius (%/decade) (right) with a real instrument compared to a perfect instrument are shown, having been linked to an estimate of the Effective Radiative Forcing due to aerosol cloud interactions (ERFaci) decadal trend. The dashed line shows the requirement determined for an instrument capable of detecting trends within 20% trend uncertainty compared to a perfect observing system. *V* and *M* denote the absolute calibration accuracies in the 3.8 μm bands for VIIRS and MODIS, respectively.